nature nanotechnology

SUPPLEMENTARY INFORMATION

https://doi.org/10.1038/s41565-018-0141-z

In the format provided by the authors and unedited.

Carbon nanotube bundles with tensile strength over 80 GPa

Yunxiang Bai[1,2,5], Rufan Zhang[1,5*], Xuan Ye[2,3,5], Zhenxing Zhu[1,2], Huanhuan Xie[1,2], Boyuan Shen[1], Dali Cai[1], Bofei Liu[4], Chenxi Zhang[1,2], Zhao Jia[1], Shenli Zhang[1], Xide Li[2,3*] and Fei Wei[1,2*]

[1]Beijing Key Laboratory of Green Chemical Reaction Engineering and Technology, Department of Chemical Engineering, Tsinghua University, Beijing, China. [2]Center for Nano and Micro Mechanics, Tsinghua University, Beijing, China. [3]Department of Engineering Mechanics, AML, Tsinghua University, Beijing, China. [4]Department of Materials Science and Engineering, Stanford University, Stanford, CA, USA. [5]These authors contributed equally: Yunxiang Bai, Rufan Zhang, Xuan Ye. *e-mail: zhangrufan@tsinghua.edu.cn; lixide@tsinghua.edu.cn; wf-dce@tsinghua.edu.cn

Supplementary Information for

Fabrication of Super-strong Carbon Nanotube Bundles with Tensile Strength over 80 GPa

Yunxiang Bai[1,3†], Rufan Zhang[1†,*], Xuan Ye[2,3†], Zhenxing Zhu[1,3], Huanhuan Xie[1,3], Boyuan Shen[1], Dali Cai[1], Bofei Liu[4], Chenxi Zhang[1,3], Zhao Jia[1], Shenli Zhang[1], Xide Li[2,3*], Fei Wei[1,3*]

[1]Beijing Key Laboratory of Green Chemical Reaction Engineering and Technology, Department of Chemical Engineering, Tsinghua University, Beijing 100084, China.

[2]Department of Engineering Mechanics, AML, Tsinghua University, Beijing 100084, China.

[3]Center for Nano and Micro Mechanics, Tsinghua University, Beijing 100084, China.

[4]Department of Materials Science and Engineering, Stanford University, Stanford, CA 94305, USA.

[†]These authors contributed equally to this work.

*Correspondence to: zhangrufan@tsinghua.edu.cn; lixide@tsinghua.edu.cn; wf-dce@tsinghua.edu.cn

This file contains the following information:

Supplementary Figures, Supplementary Tables, and Supplementary Texts.

1. Supplementary Figures

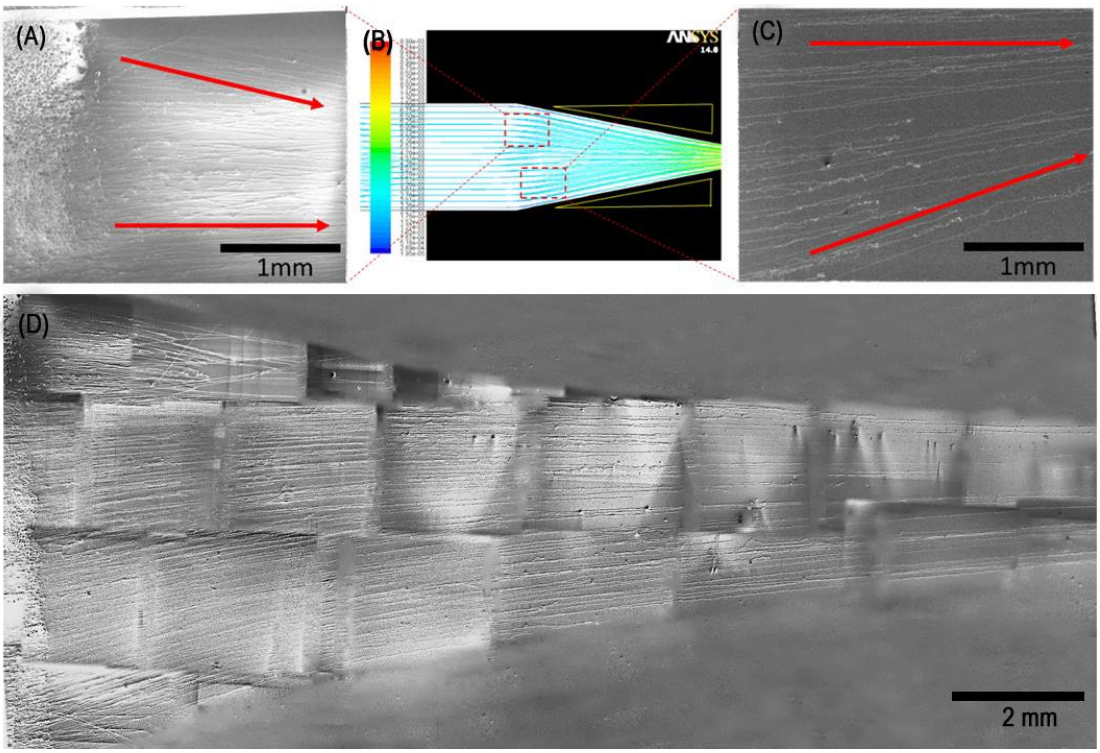

Figure S1. Mosaic SEM images of as-grown ultralong CNTs with the GFF method.

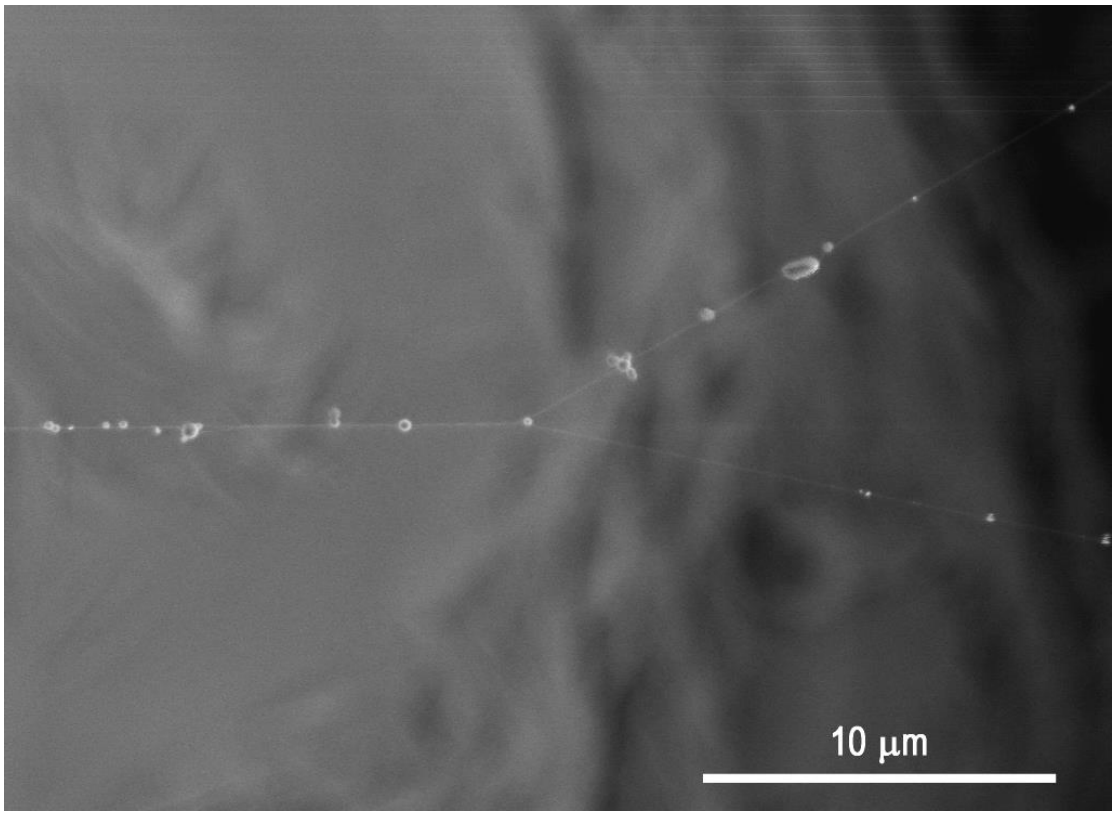

Figure S2. SEM image of a CNTB-2 decorated with TiO_2 nanoparticles.

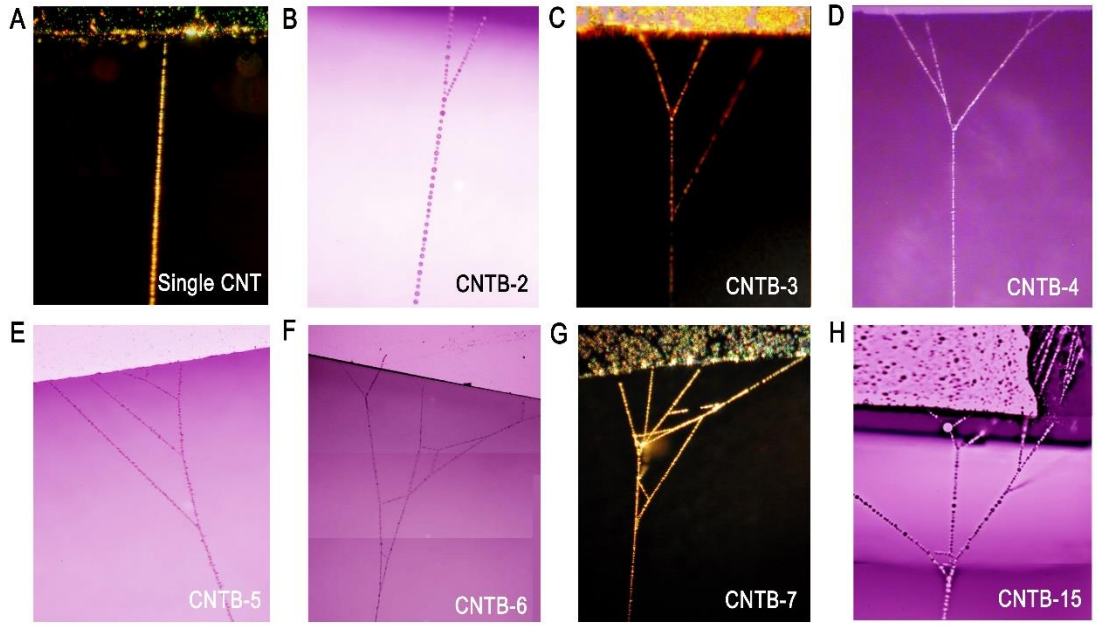

Figure S3. Optical microscopy images of a single CNT and CNTBs consisting of different numbers of CNTs.

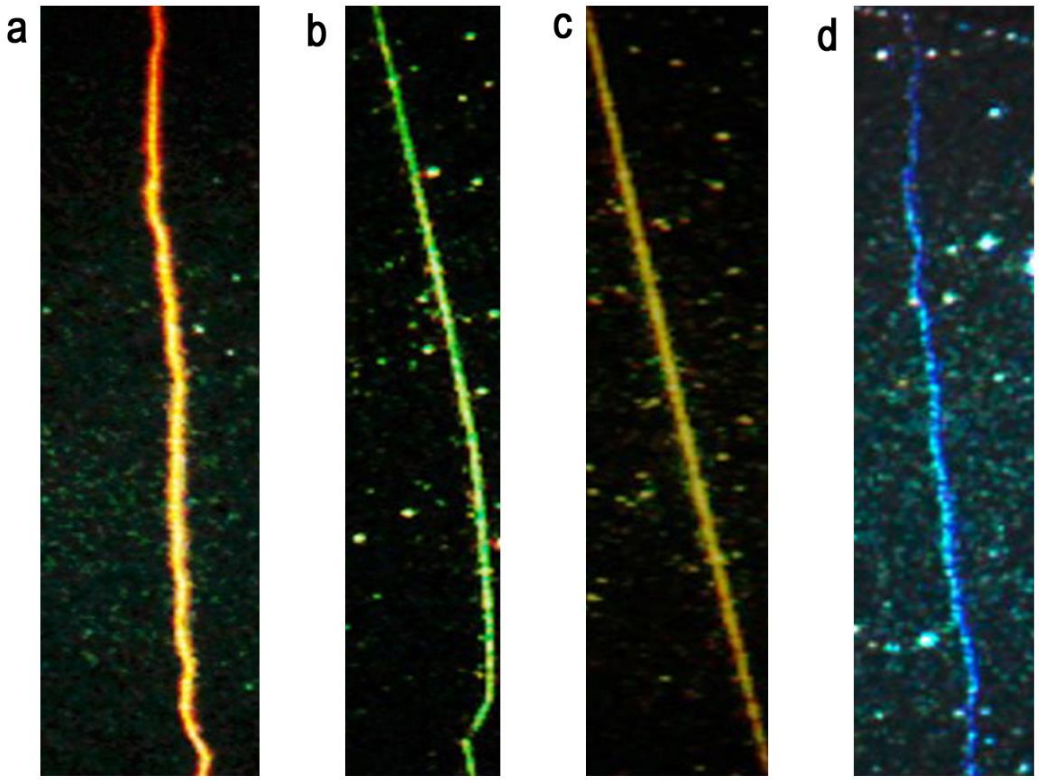

Figure S4. Resonance Rayleigh scattering images of single CNTs with different chiralities.

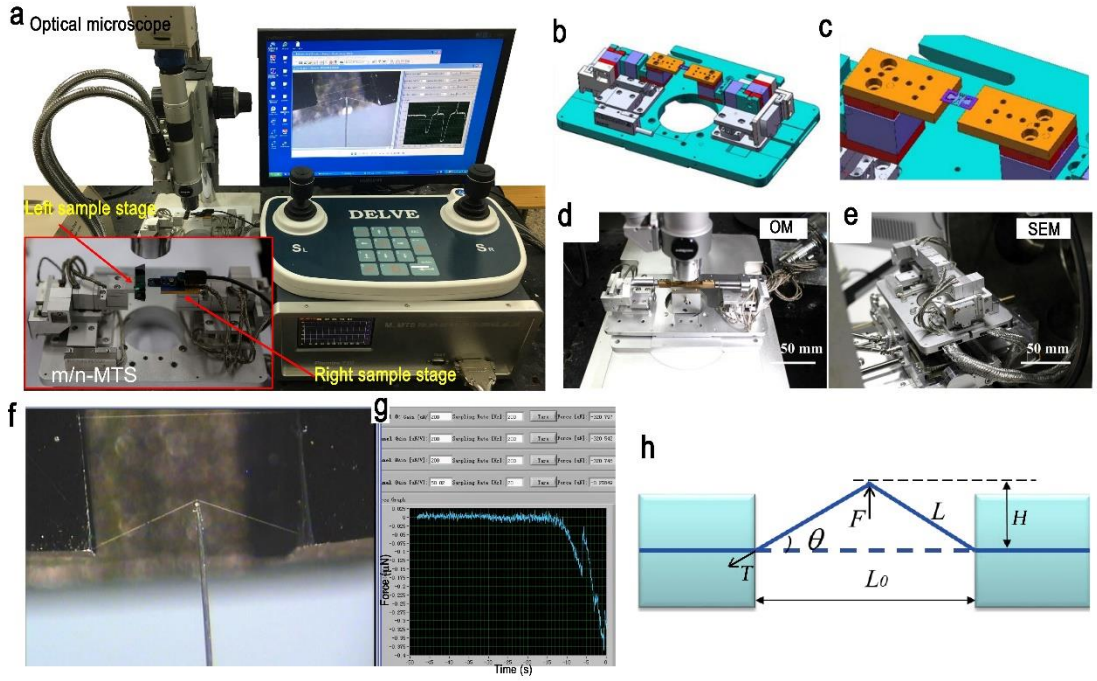

Figure S5. Mechanical measurement systems for CNTs/CNTBs. (a) Image of a m/n-MTS fixed with an optical microscope. (b) Schematic illustration showing the module composition of the mechanical measurement part in the m/n-MTS. (c) Enlargement of the central section in (b). (d) Photo of m/n-MTS under an OM. (e) Photo of m/n-MTS under a SEM. (f) Microscopic image of the tension of a suspended CNT under the OM and (g) the corresponding applied load at the center. (h) The scheme of the measurement principle. $\boldsymbol{L_0}$ is the initial length of the suspended section of a sample without tensile loading. $\boldsymbol{H}$ is the lateral displacement of the middle point of a suspended section of a CNT/CNTB, as shown in Figure S6C. $\boldsymbol{F}$ is the applied force onto the middle point of a suspended section of a CNT/CNTB. $\boldsymbol{L}$ is the length of the suspended section of a CNT/CNTB with tensile loading. $\boldsymbol{T}$ is the tensile force along the axial direction of the suspended section of a CNT/CNTB.

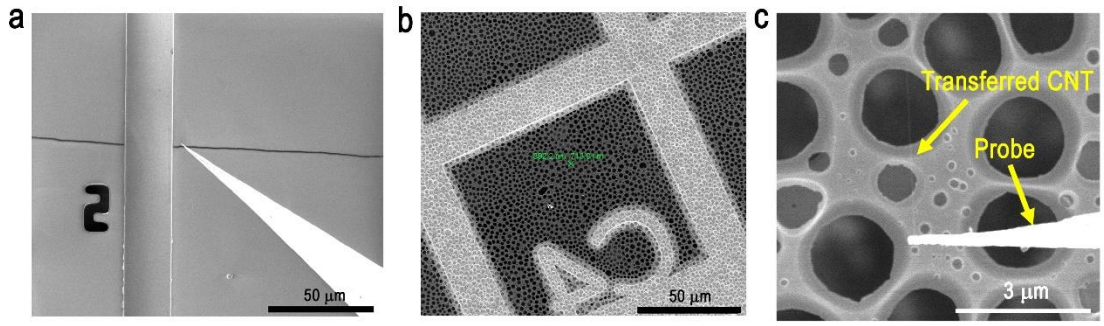

Figure S6. Transfer of CNTs/CNTBs sections onto other substrates. (a) SEM image showing the positioning of a CNT crossing a slit on the SiO_2/Si substrate. A probe can be used to manipulate the CNT. (b) and (c) SEM images with different magnification showing the transferred CNT onto a TEM grid with marks for fast and precise positioning.

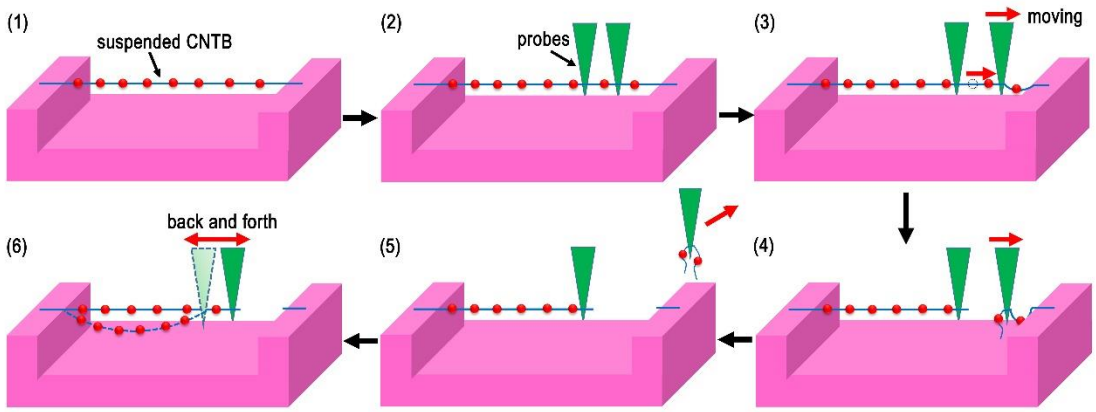

Figure S7. Schematic illustration showing the STR process using two probes.

2. Supplementary Tables

Table S1 Tensile loading of a single CNT

L_0 (mm)	d (nm)	A_1 (nm^2)				A_2 (nm^2)
1.515	2.1	2.2420				3.4636
H (mm)	F (nN)	L (mm)	T (nN)	ε	σ_1 (GPa)	σ_2 (GPa)
0.1047	19.1	1.5294	69.8	0.95	31.11	20.14
0.139	30.5	1.5403	84.4	1.67	37.64	24.37
0.1526	36.2	1.5454	91.8	2.01	40.92	26.49
0.1645	42.6	1.5503	100.4	2.33	44.79	28.99
0.1828	52.5	1.5585	111.9	2.87	49.91	32.30

0.1965	60.1	1.5651	119.6	3.31	53.35	34.53
0.2085	67.1	1.5713	126.5	3.72	56.42	36.52
0.224	81.9	1.5799	144.3	4.28	64.38	41.67
0.2383	90.7	1.5882	151.1	4.83	67.41	43.63
0.2501	100.9	1.5954	160.9	5.31	71.76	46.45
0.2582	106.2	1.6006	164.6	5.65	73.42	47.53
0.2693	116.9	1.6079	174.5	6.13	77.83	50.38
0.2782	126.6	1.6139	183.7	6.53	81.93	53.03
0.2909	137.6	1.6229	192.0	7.12	85.62	55.42
0.3058	148.6	1.6338	198.5	7.84	88.55	57.32
0.3191	163.6	1.6439	210.7	8.51	93.99	60.84
0.3314	175.0	1.6536	218.3	9.15	97.39	63.04
0.3402	184.0	1.6608	224.6	9.62	100.19	64.85
0.3551	200.4	1.6732	236.0	10.44	105.28	68.15
0.3672	213.0	1.6836	244.1	11.13	108.89	70.49
0.3756	223.7	1.6910	251.8	11.62	112.31	72.70
0.3947	242.2	1.7083	262.1	12.76	116.89	75.66
0.4054	251.9	1.7183	267.0	13.42	119.08	77.08
0.4156	262.3	1.7280	272.6	14.06	121.61	78.72
0.4245	0.0	1.7367	0.0	14.63	0.00	0.00

Table S2 Tensile loading of a CNTB-2 without STR treatment

L_0 (mm)	d (nm)		A_1 (nm^2)			A_2 (nm^2)
1.505	1.6	1.8	3.6298			4.5553
H (mm)	F (nN)	L (mm)	T (nN)	ε	σ_1 (GPa)	σ_2 (GPa)
0.0898	13.8	1.5157	58.3	0.71	16.06	12.80
0.1104	18.4	1.5211	63.5	1.07	17.49	13.93
0.1264	23.3	1.5261	70.3	1.40	19.37	15.43
0.1422	33.0	1.5316	88.9	1.77	24.48	19.51
0.1637	47.1	1.5402	110.7	2.34	30.50	24.31
0.1803	61.5	1.5476	132.0	2.83	36.38	28.99
0.1955	76.2	1.5550	151.5	3.32	41.74	33.26
0.2097	91.3	1.5623	170.0	3.81	46.84	37.32
0.2236	105.6	1.5700	185.4	4.32	51.08	40.70
0.2394	124.2	1.5793	204.8	4.94	56.43	44.97
0.2537	141.3	1.5882	221.1	5.53	60.92	48.54
0.2657	158.2	1.5961	237.6	6.05	65.47	52.17
0.2746	171.2	1.6021	249.7	6.45	68.78	54.81
0.2845	183.0	1.6090	258.7	6.91	71.28	56.80
0.2958	200.8	1.6171	274.5	7.45	75.61	60.25
0.3101	223.2	1.6278	292.9	8.16	80.68	64.29
0.325	249.6	1.6394	314.8	8.93	86.71	69.10

0.3414	275.7	1.6526	333.7	9.81	91.93	73.25
0.3488	128.9	1.6588	153.3	10.22	42.23	33.65
0.368	150.1	1.6753	170.8	11.32	47.06	37.50
0.378	159.3	1.6842	177.4	11.91	48.87	38.94
0.399	172.8	1.7035	184.4	13.19	50.81	40.49
0.4177	191.3	1.7213	197.1	14.37	54.30	43.26
0.4418	207.0	1.7452	204.4	15.96	56.31	44.87
0.4644	0.0	1.7685	0.0	17.51	0.00	0.00

Table S3 Tensile loading of a CNTB-3 without STR treatment

L_0 (mm)		d (nm)		A_1 (nm^2)	A_2 (nm^2)
1.508	1.5	2.6	1.8	6.2988	9.6211
H (mm)	F (nN)	L (mm)	T (nN)	ε	σ_1 (GPa)	σ_2 (GPa)
0.09	30.0	1.5187	126.4	0.71	20.07	13.14
0.1271	52.6	1.5293	158.2	1.41	25.13	16.45
0.1641	86.5	1.5433	203.3	2.34	32.28	21.13
0.1907	121.8	1.5555	248.4	3.15	39.43	25.82
0.2101	144.6	1.5654	269.3	3.81	42.76	28.00
0.2318	178.9	1.5777	304.4	4.62	48.32	31.64
0.2518	212.7	1.5899	335.8	5.43	53.31	34.90
0.2662	240.1	1.5992	360.6	6.05	57.24	37.48
0.2795	267.2	1.6083	384.4	6.65	61.03	39.96
0.2956	299.7	1.6197	410.6	7.41	65.19	42.68
0.3127	341.1	1.6325	445.2	8.26	70.67	46.27
0.3242	369.1	1.6415	467.2	8.85	74.18	48.56
0.3395	400.0	1.6538	487.1	9.67	77.33	50.63
0.3555	443.2	1.6672	519.6	10.56	82.48	54.00
0.3688	351.2	1.6787	399.7	11.32	63.46	41.54
0.3808	373.6	1.6894	414.3	12.03	65.78	43.07
0.3945	404.0	1.7019	435.7	12.86	69.17	45.28
0.4092	434.6	1.7158	455.6	13.78	72.32	47.35
0.4194	463.9	1.7256	477.2	14.43	75.76	49.60
0.4285	271.4	1.7345	274.7	15.02	43.61	28.55
0.4383	0.0	1.7443	0.0	15.67	0.00	0.00

Table S4 Tensile loading of a CNTB-7 without STR treatment

L_0 (mm)	d (nm)				A_1 (nm^2)	A_2 (nm^2)
1.487	3.2	2.0	1.5	1.6	13.2382	19.4308
	1.6	1.3	1.2			
H (mm)	F (nN)	L (mm)	T (nN)	ε	σ_1 (GPa)	σ_2 (GPa)
0.0906	46.7	1.4978	192.9	0.74	14.57	9.00

0.1262	90.7	1.5081	270.9	1.43	20.47	12.64
0.1572	143.0	1.5197	345.6	2.21	26.11	16.13
0.1828	197.8	1.5311	414.3	2.98	31.29	19.33
0.2049	253.2	1.5422	476.5	3.73	35.99	22.24
0.2216	301.2	1.5515	527.2	4.35	39.82	24.61
0.2397	359.8	1.5622	586.2	5.07	44.28	27.36
0.258	437.0	1.5738	666.4	5.85	50.34	31.10
0.2762	516.5	1.5861	741.5	6.68	56.01	34.61
0.2943	590.2	1.5991	801.7	7.55	60.56	37.42
0.3162	687.2	1.6157	877.8	8.67	66.31	40.97
0.3344	762.3	1.6303	929.1	9.65	70.19	43.37
0.3491	695.8	1.6426	818.4	10.48	61.82	38.20
0.3658	754.1	1.6570	854.0	11.45	64.51	39.86
0.3838	301.8	1.6733	329.0	12.54	24.85	15.35
0.3925	323.0	1.6813	345.9	13.08	26.13	16.14
0.4064	346.2	1.6945	360.9	13.97	27.26	16.84
0.4202	198.8	1.7079	202.0	14.87	15.26	9.43
0.4273	0.0	1.7149	0.0	15.34	0.00	0.00

Table S5 Tensile loading of a CNTB-2 with STR treatment

L_0 (mm)	d (nm)		A_1 (nm^2)			A_2 (nm^2)
1.468	2.2	1.6	4.0569			5.8119
H (mm)	F (nN)	L *(mm)*	T (nN)	ε	σ_1 (GPa)	σ_2 (GPa)
0.0851	9.0	1.4782	39.2	0.67	9.67	6.75
0.1107	16.4	1.4850	54.9	1.13	13.53	9.44
0.1331	26.9	1.4923	75.4	1.63	18.59	12.98
0.1502	38.9	1.4988	97.0	2.07	23.91	16.69
0.1688	52.8	1.5067	117.9	2.61	29.06	20.28
0.1845	65.1	1.5141	133.7	3.11	32.94	23.00
0.1982	79.5	1.5210	152.5	3.58	37.59	26.24
0.2127	97.2	1.5288	174.6	4.11	43.04	30.04
0.2247	114.3	1.5356	195.3	4.58	48.15	33.61
0.2403	134.0	1.5450	215.4	5.22	53.09	37.06
0.2555	156.6	1.5548	238.2	5.88	58.73	40.99
0.2755	185.5	1.5684	264.0	6.81	65.08	45.43
0.284	201.5	1.5744	279.3	7.22	68.84	48.05
0.2999	228.0	1.5862	301.5	8.02	74.31	51.87
0.3081	244.9	1.5925	316.5	8.45	78.01	54.46
0.319	262.0	1.6010	328.8	9.03	81.04	56.57
0.3333	289.1	1.6126	349.7	9.82	86.20	60.17
0.3508	322.9	1.6274	374.5	10.83	92.32	64.44
0.3649	350.3	1.6398	393.5	11.67	96.99	67.70
0.3721	364.3	1.6462	402.9	12.11	99.31	69.32

0.3811	382.1	1.6544	414.7	12.67	102.22	71.36
0.3912	401.9	1.6638	427.4	13.31	105.34	73.53
0.4	417.1	1.6722	435.9	13.88	107.46	75.01
0.4076	0.0	1.6795	0.0	14.38	0.00	0.00

Table S6 Tensile loading of a CNTB-3 with STR treatment

L_0 (mm)		d (nm)		A_1 (nm^2)	A_2 (nm^2)
1.526	2.3	1.5	1.2	5.3380	7.0529

H (mm)	F (nN)	L (mm)	T (nN)	ε	σ_1 (GPa)	σ_2 (GPa)
0.0979	8.0	1.5387	31.3	0.82	5.87	4.44
0.1417	26.9	1.5523	73.6	1.71	13.78	10.43
0.1734	51.5	1.5651	116.2	2.55	21.76	16.47
0.1949	72.5	1.5752	146.4	3.21	27.43	20.76
0.216	101.8	1.5862	186.8	3.93	34.99	26.49
0.2328	128.2	1.5956	219.7	4.55	41.15	31.14
0.258	167.9	1.6111	262.1	5.56	49.11	37.17
0.2731	195.9	1.6210	290.6	6.21	54.45	41.21
0.2937	233.8	1.6353	325.5	7.15	60.98	46.15
0.3091	268.4	1.6467	357.5	7.89	66.98	50.69
0.329	312.3	1.6620	394.4	8.90	73.88	55.92
0.3462	356.1	1.6759	430.9	9.81	80.73	61.10
0.3634	390.1	1.6904	453.6	10.76	84.98	64.32
0.377	424.6	1.7023	479.3	11.54	89.78	67.95
0.3915	452.6	1.7153	495.7	12.39	92.87	70.29
0.3986	474.1	1.7219	512.0	12.82	95.91	72.59
0.409	498.9	1.7316	528.0	13.46	98.91	74.86
0.4172	0.0	1.7394	0.0	13.97	0.00	0.00

Table S7 Tensile loading of a CNTB-7 with STR treatment

L_0 (mm)	d (nm)				A_1 (nm^2)	A_2 (nm^2)
1.496	3.2	1.7	2.2	1.4	15.8005	26.2480
	2.5	1.8	2.0			

H (mm)	F (nN)	L (mm)	T (nN)	ε	σ_1 (GPa)	σ_2 (GPa)
0.0906	17.4	1.5073	72.2	0.73	4.57	2.49
0.1279	58.9	1.5181	174.7	1.45	11.06	6.04
0.1538	104.3	1.5277	258.9	2.09	16.39	8.95
0.1812	172.8	1.5397	367.2	2.89	23.24	12.69
0.2037	242.7	1.5509	461.9	3.64	29.23	15.96
0.2223	307.7	1.5611	540.2	4.32	34.19	18.66
0.2417	392.2	1.5725	637.9	5.09	40.37	22.04
0.2553	457.0	1.5811	707.6	5.66	44.79	24.45

0.2682	522.8	1.5896	774.7	6.23	49.03	26.77
0.2842	611.3	1.6007	860.7	6.97	54.48	29.74
0.2964	686.9	1.6095	932.5	7.56	59.02	32.22
0.3152	801.8	1.6238	1032.7	8.51	65.36	35.68
0.3327	911.3	1.6377	1121.5	9.44	70.98	38.75
0.3472	996.3	1.6497	1183.4	10.24	74.90	40.89
0.3603	1082.8	1.6609	1247.9	10.99	78.98	43.12
0.3744	1188.1	1.6733	1327.5	11.82	84.02	45.87
0.3869	1276.8	1.6846	1389.9	12.58	87.96	48.02
0.3998	666.9	1.6966	707.5	13.38	44.78	24.45
0.4073	0.0	1.7038	0.0	13.86	0.00	0.00

Note: $\boldsymbol{L_0}$ is the initial length of the suspended section of a sample without tensile loading. $\boldsymbol{d}$ is the diameter of single CNTs. $\boldsymbol{A_1}$ is the cross-sectional area of CNTs/CNTBs without including the hollow parts in CNTs, $\boldsymbol{A_1}=\pi t\Sigma d_i$, where d_i is the diameter of the ith CNT and t is the CNT wall thickness (0.34 nm); $\boldsymbol{A_2}$ is the cross-sectional area of CNTs/CNTBs including the hollow parts in CNTs, $\boldsymbol{A_2}=\pi\Sigma\left(\frac{d_i}{2}\right)^2/0.9069$, where d_i is the diameter of the ith CNT, 0.9069 is the maximum possible packing density of cylinders (it should be noted here that for number of CNTs in a CNTB smaller than 3, we did not take the 0.9069 into consideration), $\boldsymbol{H}$ is the lateral displacement of the middle point of a suspended section of a CNT/CNTB, as shown in Figure S6C. $\boldsymbol{F}$ is the applied force onto the middle point of a suspended section of a CNT/CNTB. $\boldsymbol{L}$ is the length of the suspended section of a CNT/CNTB with tensile loading. $\boldsymbol{T}$ is the tensile force along the axial direction of the suspended section of a CNT/CNTB. $\boldsymbol{\varepsilon}$ is the tensile strain of the suspended section of a CNT/CNTB. $\boldsymbol{\sigma_1}$ and $\boldsymbol{\sigma_2}$ are the tensile stress of the sample based on $\boldsymbol{A_1}$ and $\boldsymbol{A_2}$, respectively.

3. Supplementary Texts

Text S1. The deposition mechanism of TiO_2 nanoparticles on suspended CNTs

As has been reported previously[1], the deposition of TiO_2 nanoparticles on suspended CNTs was conducted in a vapor phase hydrolysis of $TiCl_4$, which is a highly volatile metal halide and can forms misty smog of TiO_2 and HCl upon contact with

humid air[2]. Tiny TiO_2 nanoparticles would nucleate on the CNTs immediately after $TiCl_4$ vapor got into contact with suspended CNTs, which also played a role of templates in tailoring the size of TiO_2 nanoparticles[3]. As the pristine CNTs are hydrophobic[4] while the TiO_2 nanoparticles are hydrophilic[5], thus the following formed TiO_2 in the gas phase prefers to attach on the TiO_2 nucleates. The –OH groups on the surface of TiO_2 nanoparticles also catalyzed $TiCl_4$ hydrolysis[6], resulting in the vapor phase epitaxial growth of the pre-existing TiO_2 nanoparticles. The small TiO_2 nanoparticles attached on the outer wall of the suspended CNTs gradually grew larger and wrapped the CNTs with the continuously growth. Meanwhile, a large amount of newly nucleated TiO_2 nanoparticles formed and adhered to the suspended CNTs. Therefore, small and large TiO_2 nanoparticles coexist on the suspended CNTs. The interactions between the TiO_2 nanoparticles and the CNTs is dominated by van der Waals force[3,7], which is much smaller than the tensile strength of pristine CNTs.

Text S2. The effect of TiO_2 nanoparticles on the Raman spectra and mechanical properties of CNTs

As shown in Figure 1k in the main text, the TiO_2 nanoparticles are just separately distributed on the suspended CNTs, without forming a continuous coating layer. Between the adjacent particles are the pristine CNT sections which still preserve their original properties. There is only van der Waals interaction between TiO_2 nanoparticles and CNTs. It is found that the Raman spectra of a suspended CNT with TiO_2 nanoparticles is almost completely identical with that without TiO_2 nanoparticles[1],

clearly confirming that the structures and properties of CNTs are not affected by the TiO_2 nanoparticles. As for the mechanical properties of CNTs, it is straightforward and obvious that the tensile strength and breaking strain of a CNT are not influenced by the deposition of discrete TiO_2 nanoparticles under tensile stretching, which has already by confirmed by our previous work[8] and will also be confirmed in the following discussion in Text S5 and S6 below.

Text S3. The one-by-one breaking of CNTs in a bundle

Take the CNTB-2 shown in Figure 2a in the main text as an example, it is evident that, with the strain increased from zero to *ca*. 9.5% (which is the critical breaking strain for this CNTB-2), the tensile stress has a steady increase. Then, there is a sharp decrease of the tensile stress, indicating that one of the two CNTs is broken, making the apparent tensile stress of the CNTB-2 suddenly decrease from *ca.* 91.9 GPa to *ca.* 42.2 GPa. With the strain increased from *ca.* 10% to *ca.* 16%, the increase of the apparent tensile stress of the CNTB-2 becomes slower due to the breaking of one component in the CNTB-2 and the inelastic deformation of the remaining CNT under large tensile strains. With the further increase of the strain > 16%, the CNTB-2 is completely broken. Other CNTBs, such as CNTB-3 and CNTB-7, also exhibit similar multi-stage stress-strain features.

Text S4. The introduction of initial strain/stress in suspended CNTs or CNTBs

There are two reasons for the introduction of initial strain/stress in suspended

CNTs or CNTBs. The first reason roots in the non-uniform van der Waals interaction between the suspended CNTs/CNTBs and the substrate. During the gas-flow-directed growth process, when the floating CNTs/CNTBs land onto the substrate with slits, for the unsuspended sections, the van der Waals interaction is uniformly distributed on the whole unsuspended sections. However, for the suspended sections laying across the slits, only the two ends are dragged by the van der Waals interaction from the substrate, thus introducing an initial strain/stress to the suspended CNTs/CNTBs. The second reason for the initial strains lies in the formation of the CNTBs. As shown in Figure 1a, c and m, the flowing CNTs are easy to assemble with each other due to the van der Waals interaction between them. Thus, different initial strains are introduced in the formation process of CNTBs.

Text S5. The sliding of TiO_2 nanoparticles along CNTBs

Chen et al. has confirmed that for CNTs buried in matrix with limited length, if the interface strength between CNTs and matrix is weak, the CNTs cannot be broken under tensile stretching, but be completely pulled out from the matrix[9]. Similarly, for CNTs coated with discrete TiO_2 nanoparticles, because of the weak van der Waals interaction between TiO_2 nanoparticles and CNTs, the CNTs can also be pulled out from the TiO_2 nanoparticles when applying a force larger than the interface strength between them. It has been confirmed that the interaction between TiO_2 nanoparticles and CNTs is van der Waals force[3,7], which is much smaller than the tensile strength of pristine CNTs. For example, it was calculated that the TiO_2/CNT interaction is about -0.65 eV[10], while the C=C bond energy is 6.344 eV, which is much higher than the TiO_2/CNT interaction.

Moreover, the small contact area between CNTs and individual TiO_2 nanoparticles is another important beneficial factor which favors the sliding of TiO_2 nanoparticles along the CNTs. The diameters of TiO_2 nanoparticles range from several nanometers to several hundred nanometers, thus the contact length between CNTs and individual TiO_2 nanoparticles is also in a similar range. It has been reported that the specific linear friction between a CNT and SiO_2/Si substrate is about 5 pN/nm[11]. Because of the weak van der Waals interaction between CNTs and TiO_2 nanoparticles, if we consider the specific linear friction between a CNT and TiO_2 nanoparticle to be of a similar value of 5 pN/nm, for a TiO_2 nanoparticle with diameter of 500 nm, the friction between a CNT and this TiO_2 nanoparticle is only 2.5 nN, a value much lower than the highest tensile force that a CNT can endure (usually several hundred nN). Therefore, if applying an external force which is larger than the interaction between the TiO_2 nanoparticles and CNTs, the deposited TiO_2 nanoparticles can move, slide or rotate along the CNTs, without changing the structures of CNTs.

Here we take a CNTB-2 consisting of two single CNTs as an example to investigate the sliding of TiO_2 nanoparticles along CNT bundles. As shown in Figure 4d in the main text of the paper, because of the non-uniformity of the initial strains in the CNTB-2, when stretched along the axial direction of the CNTB-2, the forces on the two sides of TiO_2 nanoparticles are unequal due to the different tensile strains at different sections (Figure 4d (1) and (2)). With the increase of the total tensile strain of the CNTBs, the force difference between the TiO_2 nanoparticles also increases, which will finally be larger than the interaction between the TiO_2 nanoparticles and the CNTs

and thus cause the sliding of TiO_2 nanoparticles along the CNTs (Figure 4d (3)). In this way, the tensile strain difference between the CNTB components will be released and a more uniform initial strain distribution can be obtained after releasing the external forces (Figure 4d (4)). Besides, the weak van der Waals interaction between adjacent CNTs is also a crucial factor in the above sliding process of TiO_2 nanoparticles along the CNTs.[12] Therefore, the non-uniform tensile strain of different CNTs in a CNTB on the two sides of a TiO_2 nanoparticle can easily drive the sliding of TiO_2 nanoparticle along the CNTB.

On the other hand, one may also concern the slippage of suspended CNTs during the stretching of them with a probe. As shown in Figure 1j and 1q in the main text of the paper, the un-suspended sections of the CNTs/CNTBs are fixed on the SiO_2/Si substrate. Even for a weak interface strength, if the interface length is large enough, the total interface friction between CNTs and the matrix will still be high enough to cause the CNT breaking. Kong *et al.* calculated that specific linear friction between a CNT and SiO_2/Si substrate is about 5 pN/nm[11]. As shown in the Figure 1q, the length of the unsuspended section of CNTs is on the order of centimeters, which means that, the total friction would be higher than 50000 nN, which is about two orders of magnitude higher than the highest tensile force a single CNT could endure (usually several hundred nN). Thus, the friction between CNTs and substrate would firmly fix the two ends of the suspended CNTBs from slippage during the stretching of them.

Text S6. The enforcement effect of TiO_2 nanoparticles on the intertube interaction

between CNTB components

It is widely known that, in order to increase the mechanical strength of a rope, one must improve the load transfer between the filaments of the rope so that the full rope cross-section would be participating in the loading-bearing up to the intrinsic filaments' breaking strength. As for the CNT bundles, the CNTs can easily separate from or slide on each other due to the weak van der Waals interaction between them, resulting in a largely decreased shear modulus of CNT bundles, which is also a major obstacle in the fabrication of macroscopic CNT fibers. Introducing stable connections between CNTs, without significantly degrading their Young's modulus and tensile strength in the process, is of significant importance in the fabrication of CNT fibers. Previous studies mainly employing electron-beam irradiation inside a TEM to introduce intertube crosslinks between adjacent CNTs with bundles[13,14]. Although a stable intertube connection was obtained and the bending modulus of the CNTBs were increased, a lot of structural defects were also introduced into the CNTs which seriously decreased the tensile strength of these CNTBs.

In comparison, the TiO_2 nanoparticles used here exhibit obvious advantages in reinforcing the intertube connection insides a CNTB. On the one hand, as shown in Figure 4e in the main text, the TiO_2 nanoparticles can firmly fixed the discrete CNTs into a bundle but still allow the controllable intertube sliding to achieve a more uniform initial strain distribution, preventing the separation of the CNTs from each other. Thus, the intertube load transfer can be well reserved and a higher tensile strength of the ultralong CNTBs can be obtained. On the other hand, as discussed above, the discretely

deposited TiO_2 nanoparticles do not affect the intrinsic tensile strength of pristine CNTs, but can greatly increase the utilization coefficient of single CNTs' strength when assembled in the bundles. Therefore, the TiO_2 nanoparticles deposited CNTBs provide an ideal platform to study the mechanical strength of ultralong CNTBs.

Text S7. The effect of CNT chirality on the tensile strength of CNTBs.

Generally speaking, the CNT chirality (*i.e.*, (n, m) value) has almost no effect on the tensile strength of CNTBs, which can be understood from the following two aspects: i) the effect of (n, m) distribution on the tensile strength of individual CNTs, and ii) the effect of (n, m) distribution on the inter-tube interaction of CNTs. Firstly, it has been widely accepted that the chirality of CNTs has no effect on their mechanical properties,[15-17] which means that the CNT (n, m) distribution has no effect on the tensile strength of individual CNTs. Secondly, as for the impact of chirality on the intershell interaction of CNTs, we have made a detailed discussion in our previous work about the macroscale superlubricity on centimeters long double-walled CNTs (DWCNTs).[12] Here we take a DWCNT as an example to give a brief discussion. DWCNTs can be viewed as concentrically curved bilayer graphene sheets and the concept of the lattice matching between the carbon network layers can be therefore extended to understand the wall-wall interactions of DWCNTs. For DWCNTs, the (n, m) index of different shells are independent with each other. Only when the inner and outer shells meet the requirement of armchair@amchair or zigzag@zigzag that meet the lattice matching can they satisfy the AB stacking for commensurate contact as two graphite sheets.[18-23] The commensurate configuration of the AB stacked bilayer graphene has the largest

interactional energies compared with the other incommensurate configurations[22,23], which means that the intershell friction will has a sharp increase for the commensurate bilayer graphene[23]. When the inner and outer shells of DWCNTs have the configuration as armchair@amchair or zigzag@zigzag, they meet the lattice matching, or commensurate configuration, and in this case the interactional energies or frictions between the inner and outer shells of DWCNTs are much larger than those of any other configurations due to the AB lattice matching. Obviously, most of the chirality of inner and outer shells in DWCNTs can hardly meet the above requirement simultaneously. Therefore, for most DWCNTs, the two shells are incommensurate and keep in superlubricity state. Similarly, for the individual CNTs in a bundle, the chirality has little impact on their inter-CNT friction. In conclusion, the CNT (n, m) distribution has almost no effect on the tensile strength of CNTBs.

Text S8. The Weibull distribution of the tensile strength of CNTs and the Daniels effect

We find that the strength of single CNTs obeys the Weibull distribution, which has been widely employed to describe the strength distribution of single filaments and carbon fibers[24-28]. On the one hand, for the general CNTs, the strength distribution for single CNTs is usually highly dispersive due to the existence of structural defects. On the other hand, even for ultralong defect-free CNTs, as discussed above, the apparent strength (*i.e.*, *r*-strength) distribution of single CNTs in CNTBs is also dispersive due to the nonuniformity of the initial strains/stresses when bundled together. Hence, it implies that the strength distribution of single CNTs fits well the prerequisites of the

weakest-connection theory which is applied to express the strength distribution of single filaments, referring to the cases that, i) the breaking of single filament always takes place at the weakest cross section of the filament; ii) the tensile strength is always a positive value for whatever filament length; iii) the breaking probability *F(σ)* of single filament is the monotonic increasing function of its tensile loading σ[29]. Therefore, the strength of single CNTs obeys the Weibull distribution.

For single CNTs of unit length, the two-parameter Weibull distribution can be written as:

$$F(\sigma) = 1 - \exp[-(\sigma/\eta)^{\beta}] \tag{1}$$

, with mean value of

$$E(\sigma) = \eta\Gamma(1 + 1/\beta) \tag{2}$$

and variance of

$$D(\sigma) = \eta^2[\Gamma(1 + 2/\beta) - \Gamma^2(1 + 1/\beta)] \tag{3}$$

, where $F(\sigma)$ is the breaking probability of single CNTs under a stress no greater than σ, $\Gamma(\cdot)$ is the gamma function, η and β refers to the scale parameter and shape parameter of the Weibull distribution, respectively.

In order to obtain the value of β and η, the Weibull distribution function can also be written as

$$\ln(-\ln[1 - F(\sigma)]) = \beta\ln\sigma - \beta\ln\eta \tag{4}$$

, $F(\sigma)$ can be calculated from $F(\sigma) = n/(N_0 + 1)$, where N_0 is total number of single CNTs being measured, and n is the number of CNTs being broken under tensile stress σ. Thus β and η can be obtained from the slop and intercept of the fitting line of Equation (4).

In Figure 5a, the two lines are just the fitting line of Equation (4).

In Figure 5a, the CV is the coefficient of variation (also called coefficient of dispersion), which is the ratio of the variation to the mean value of single CNT strength,

$$CV = \frac{\sqrt{D(\sigma)}}{E(\sigma)} = \frac{\sqrt{\Gamma(1+2/\beta)}}{\Gamma^2(1+1/\beta)} - 1 \tag{5}$$

Daniels effect refers to the phenomenon that the mean tensile strength of a bundle of threads decreases with the increase of thread number. For bundles consisting of a large number (n) of single filaments with strength that obeys the Weibull distribution, the tensile strength of the bundles obeys the normal distribution with the mean value expressed as

$$E_\sigma(n) = \sigma_0[1 - F(\sigma_0)] + \frac{c_n}{n} \tag{6}$$

, where the definition of $F(\sigma_0)$ is the same with that defined in Weibull distribution, *i.e.*, the breaking probability of single CNTs under a stress no greater than σ_0. The parameter c_n can be obtained from

$$c_n = 0.966an^{\frac{1}{3}} \tag{7}$$

, where a is a parameter that can be deduced from the boundary condition n=1. The parameter σ_0 (defined as critical strength here) is the solution of

$$\max(\sigma[1 - F(\sigma)]) \tag{8}$$

. The two curves in Figure 5b are just calculated from Equation (6), from which it can be clearly seen that the mean tensile strengths ($E_\sigma(n)$) of bundles decreases with the n increasing. However, for a given CNT bundles, as the values of σ_0 and $F(\sigma_0)$ are fixed, so the value variation of $E_\sigma(n)$ only depends on the value of $\frac{c_n}{n}$, which decrease with

the increase of n and finally reach zero. Thus, the value of $E_\sigma(n)$ approaches a fixed number when the value of n is large enough. As for the experimentally measured data shown in Figure 5b, we can see that these date fitted very well with the theoretically calculated data. As for the curve surface shown in Figure 5c, it is calculated based on Equation (8).

Supplementary References:

1 Zhang, R. *et al.* Optical visualization of individual ultralong carbon nanotubes by chemical vapour deposition of titanium dioxide nanoparticles. *Nat. Commun.* **4**, 1727, (2013).

2 Rigo, M., Canu, P., Angelin, L. & Della Valle, G. Kinetics of TiCl4 hydrolysis in a moist atmosphere. *Ind Eng Chem Res* **37**, 1189-1195, (1998).

3 Georgakilas, V. *et al.* Decorating carbon nanotubes with metal or semiconductor nanoparticles. *J. Mater. Chem.* **17**, 2679-2694, (2007).

4 Hummer, G., Rasaiah, J. C. & Noworyta, J. P. Water conduction through the hydrophobic channel of a carbon nanotube. *Nature* **414**, 188-190, (2001).

5 Sakai, N., Wang, R., Fujishima, A., Watanabe, T. & Hashimoto, K. Effect of ultrasonic treatment on highly hydrophilic TiO2 surfaces. *Langmuir* **14**, 5918-5920, (1998).

6 Li, Y., Fan, Y. & Chen, Y. A novel method for preparation of nanocrystalline rutile TiO2 powders by liquid hydrolysis of TiCl4. *J. Mater. Chem.* **12**, 1387-1390, (2002).

7 Eder, D. & Windle, A. H. Morphology control of CNT-TiO_2 hybrid materials and rutile nanotubes. *J. Mater. Chem.* **18**, 2036-2043, (2008).

8 Zhang, R. *et al.* Superstrong ultralong carbon nanotubes for mechanical energy storage. *Adv. Mater.* **23**, 3387-3391, (2011).

9 Chen, Y. L., Liu, B., He, X. Q., Huang, Y. & Hwang, K. C. Failure analysis and the optimal toughness design of carbon nanotube-reinforced composites. *Compos. Sci. Technol.* **70**, 1360-1367, (2010).

10 Thuy Nguyen, M. *et al.* A study on carbon nanotube titanium dioxide hybrids: experiment and calculation. *Adv. Nat. Sci.: Nanosci. Nanotechnol.* **5**, 045018, (2014).

11 Son, H. *et al.* Strain and friction induced by van der Waals interaction in individual single walled carbon nanotubes. *App. Phys. Lett.* **90**, 253113, (2007).

12 Zhang, R. *et al.* Superlubricity in centimetres-long double-walled carbon nanotubes under ambient conditions. *Nat. Nanotechnol.* **8**, 912-916, (2013).

13 Kis, A. *et al.* Reinforcement of single-walled carbon nanotube bundles by intertube bridging. *Nat. Mater.* **3**, 153-157, (2004).

14 Peng, B. *et al.* Measurements of near-ultimate strength for multiwalled carbon nanotubes and irradiation-induced crosslinking improvements. *Nat. Nanotechnol.* **3**, 626-631, (2008).

15 Zhang, R., Zhang, Y. & Wei, F. Controlled synthesis of ultralong carbon nanotubes with perfect

structures and extraordinary properties. *Acc. Chem. Res.* **50**, 179-189, (2017).

16 Qian, D., Wagner, G. J., Liu, W. K., Yu, M.-F. & Ruoff, R. S. Mechanics of carbon nanotubes. *Appl. Mech. Rev.* **55**, 495-533, (2002).

17 Zhang, R., Zhang, Y. & Wei, F. Horizontally aligned carbon nanotube arrays: growth mechanism, controlled synthesis, characterization, properties and applications. *Chem. Soc. Rev.* **46**, 3661-3715, (2017).

18 Wen, Q. *et al.* 100 mm Long, Semiconducting Triple-walled Carbon Nanotubes. *Adv. Mater.* **22**, 1867-1871, (2010).

19 Ding, F., Harutyunyan, A. R. & Yakobson, B. I. Dislocation theory of chirality-controlled nanotube growth. *Proc. Natl. Acad. Sci. USA* **106**, 2506-2509, (2009).

20 Liu, Z. *et al.* Observation of microscale superlubricity in graphite. *Phys. Rev. Lett.* **108**, 205503, (2012).

21 Erdemir, A. & Martin, J. M. *Superlubricity* (Elsevier, Amsterdam, 2007).

22 Xu, Z., Li, X., Yakobson, B. I. & Ding, F. Interaction between graphene layers and the mechanisms of graphite's superlubricity and self-retraction. *Nanoscale* **5**, 6736-6741, (2013).

23 Dienwiebel, M. *et al.* Superlubricity of graphite. *Phys. Rev. Lett.* **92**, 126101, (2004).

24 Nakagawa, T. & Osaki, S. The discrete Weibull distribution. *IEEE Trans. Rel.* **24**, 300-301, (1975).

25 Cohen, A. C. Maximum likelihood estimation in the Weibull distribution based on complete and on censored samples. *Technometrics* **7**, 579-588, (1965).

26 Weibull, W. A statistical distribution function of wide applicability. *J. Appl. Mech.* **18**, 293-297, (1951).

27 Chi, Z., Chou, T. W. & Shen, G. Determination of single fibre strength distribution from fibre bundle testings. *J. Mater. Sci.* **19**, 3319-3324, (1984).

28 Zhou, Y., Wang, Y., Xia, Y. & Jeelani, S. Tensile behavior of carbon fiber bundles at different strain rates. *Mater. Lett.* **64**, 246-248, (2010).

29 Zhang, Y., Wang, X., Pan, N. & Postle, R. Weibull analysis of the tensile behavior of fibers with geometrical irregularities. *J. Mater. Sci.* **37**, 1401-1406, (2002).